The TOP counter of Belle II: status and first results

Umberto Tamponi, on behalf of the Belle II TOP group

INFN - Sezione di Torino, 10124 Torino

Abstract

High-efficiency and high-purity particle identification are fundamental requirements for the success of the Belle II experiment, whose main goal is to explore new-physics scenarios in the CP-violating decays of B mesons. To achieve the required particle identification performance, Belle II utilises a Time-Of-Propagation (TOP) counter in the central barrel region. This unique device consists of 16 bars of fused silica that act simultaneously as radiator and as light guide for the Cherenkov light. Unlike in the DIRC detector, the particle identification mostly relies on measuring the time of propagation of the Cherenkov light in the radiator rather than its purely geometrical patterns. In these proceedings, we present a general overview of the status of the TOP counter, including the estimation of the time resolution, the calibration strategies and performance, and the first results obtained in the commissioning phase, both using cosmic rays and e^+e^- collision events collected during the *phase II* pilot run of the Belle II experiment. These are the first measurements of the particle identification performance of a time-of-propagation detector in a HEP experiment.

Keywords: particle identification; BelleII; TOP; Cherenkov detectors;

1. Overview

The Belle II experiment [1] at the SuperKEKB collider aims to collect 50 ab^{-1} of e^+e^- collisions at the $\Upsilon(4S)$ and the nearby bottomonium resonances $\Upsilon(3S, 5S, 6S)$ to perform precision measurements of rare B meson decays, search for signatures of new physics in the dark sector, and study the spectroscopy of exotic hadrons [2].

The first stage of data-taking, a pilot run called *phase II*, started in April 2018 and lasted until July. A total luminosity of about 0.5 fb^{-1} was collected during this period. All sub-detectors were installed during the data taking with the exception of the inner silicon tracker, that was almost completely replaced by beam-background monitoring sensors. Only one eighth of the inner tracker was installed for commissioning purposes. The phase II dataset has been used to commission the experiment, perform the early calibration and determine the initial performance of each sub-detector. In the following, we discuss, in detail, the results of the commissioning of the Time-Of-Propagation (TOP) counter.

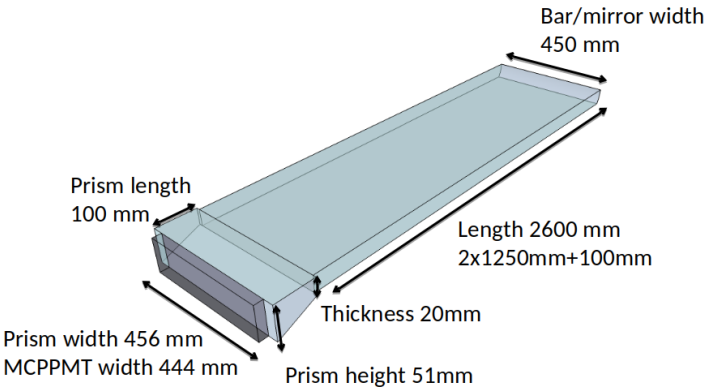

Figure 1: A schematic of one of the 16 modules of the TOP detector. The junctions between the two bar sections and between the bar and the mirror section are not shown.

2. The TOP counter

The TOP counter of the Belle II experiment is the only operational time-of-propagation Cherenkov counter [3, 4, 5, 6]. *Phase II* is therefore the first attempt to perform particle identification with such a device in a collider experiment. It is composed of sixteen identical modules arranged around the interaction point in a barrel-like geometry. A schematic for one module is given in Figure 1. Each module is composed of four parts glued together: two fused silica bars of dimension $(125 \times 45 \times 2)$ cm acting as the Cherenkov radiator, a mirror located at the forward end of the bar, and a 10 cm long prism that couples the bar to an array of micro-channel-plate photomultiplier tubes (MCP-PMTs) [7, 8]. Thanks to the high average refractive index ($n = 1.44$ at 405 nm) of the fused silica, some of the Cherenkov radiation emitted by the particles crossing the radiator remains trapped by total internal reflection, propagating to the MCP-PMT array. Having a pixel size of approximately 5.5×5.5 mm and a transit time spread of less than 50 ps, the MCP-PMTs provide a coarse measurement of the photon positions and a very precise measurement of their detection time. The photo-electron detection time, measured with respect to the initial e^+e^- collision, can be decomposed into two contributions: the time of flight of the charged particle from the

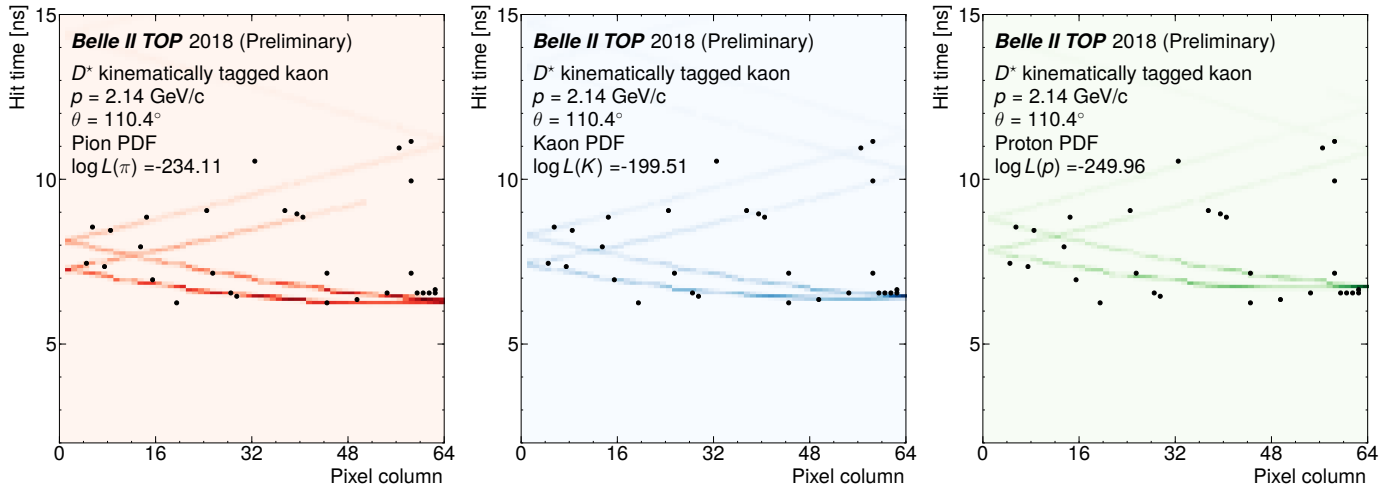

Figure 2: Space-time distribution of the hits associated to a kaon candidate track selected in the phase II data using the $D^\star$ tag described in the text. The x-axis represents the position of the pixel along the transverse dimension of the bar, while the y-axis represents the detection time, with respect to the most probable bunch crossing. The black points represent the observed hits, while the smooth distribution is the expected PDF for a pion (*left*), a kaon (*center*) or a proton (*right*) of same momentum.

interaction point to the TOP counter, and the time of propagation of the Cherenkov light inside the fused silica. The latter depends on the direction and momentum of the incoming particle, which are measured by the tracking system, and on the Cherenkov angle. The TOP counter therefore provides a combined measurement of both time of flight and Cherenkov angle.

The particle identification information is extracted by comparing the distribution of the time of arrival of the photons in each of the 512 channels with the expected Probability Density Functions (PDFs) for six particle hypotheses (e, μ, π, K, p, d) [9]. The six corresponding likelihood values are then stored, and their ratios are used to assign identification probabilities. MC simulations show that a kaon identification efficiency of 90% can be achieved while keeping the pion fake rate below 5% in the momentum region between 0.5 and 2 GeV/c [2].

3. First results using a pure sample of kaons

The early run with the TOP was overall successful: the subdetector took part in more than 90% of the data taking, with a 2.5% fraction of dead channels, and its particle identification capabilities were demonstrated for the first time.

The TOP particle identification capabilities were studied in data by selecting pure samples of pions, kaons, and protons reconstructed in the decay chains $D^{\star+} \to D^0\pi^+ \to K^-\pi^+\pi^+$, $K_s \to \pi^+\pi^-$, and $\Lambda \to p\pi^-$ [1]. These proceedings will focus on the kaon/pion separation power and on the pion fake rates, determined using the $D^{\star+}$ and the K_s decays in the first 90 pb^{-1} of data. All the results presented are obtained with preliminary, severely limited time calibrations and without any geometrical alignment. Precise numerical results are therefore not presented here.

The $D^{\star+}$ reconstruction begins with selecting $D^0 \to K^-\pi^+$ candidates. The D^0 is reconstructed from track pairs of opposite charge pointing to the primary interaction point. The kaon mass hypothesis is assigned to one track and that of the pion to the other one, without using any particle identification information. The kaon candidate is required to be within the TOP acceptance. After applying a kinematic fit to constrain the track to a common vertex, most of the combinatorial background is discarded by requiring the D^0 candidate to have a mass between 1.85 GeV/c^2 and 1.88 GeV/c^2, corresponding to a 2.5σ window around the D^0 peak. The remaining D^0 candidates are then combined with an additional track of charge opposite to the kaon to reconstruct the $D^{\star+}$ candidates. Again, a vertex-constrained kinematic fit is performed and we require the mass difference between the $D^{\star+}$ and the D^0 candidate to be between 143.6 MeV/c^2 and 147.6 MeV/c^2. Finally the combinatorial background is further suppressed by requiring the $D^{\star+}$ candidates to have a momentum in the center-of-mass frame of greater than 2.5 GeV/c^2. The result of this procedure is a small, but pure sample of kaons with less than 5% contamination from other particles, mostly pions.

Using this pure kaon sample one can clearly visualize how the Cherenkov ring is reconstructed in a coordinate-time space by the TOP counter. Figure 2 shows the MCP-PMT hit timing distribution associated to a kinematically tagged kaon, compared with the PDFs expected for a pion, kaon or proton of the same momentum and angle.

For each kinematically tagged kaon, we calculate the likelihood values $\mathcal{L}_\pi$ and $\mathcal{L}_K$ for the pion and kaon hypotheses by comparing the observed time and spacial distribution of the detected photons with the expected ones. Figure 3 shows the log-

[1] Charge conjugation is implied for all processes discussed in this paper.

likelihood difference $\Delta LL = \log \mathcal{L}_K - \log \mathcal{L}_\pi$ for this sample. The distribution is shifted towards positive values, indicating that the TOP counter is more likely to identify kaons as kaons rather than pions, as expected.

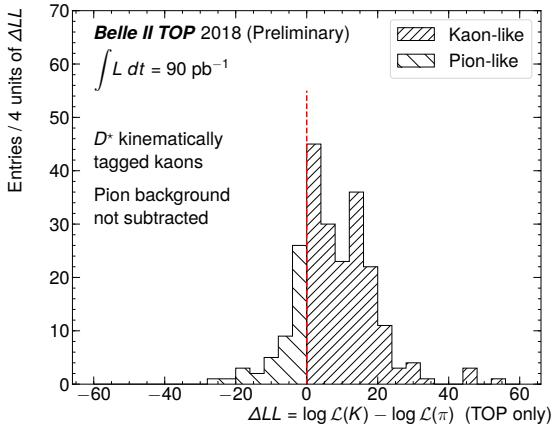

Figure 3: Difference between $\log \mathcal{L}_K$ and $\log \mathcal{L}_\pi$ for kaons tagged by the $D^{\star+} \to D^0[\to K^-\pi^+]\pi^+$ decay. Only the TOP detector is used to calculate the likelihood values.

4. First results using pure samples of pions

To measure the probability $\mathcal{P}(\pi \to X)$ for a pion to be misidentified as another particle X, we reconstruct the $K_s \to \pi^+\pi^-$ decay, applying the same loose criteria used to select the tracks for the $D^{\star+}$ reconstruction. In addition, one of the two pion candidates is required to be within the TOP acceptance (*probe*), while no selection is applied to the other track. We then study the yield of K_s as a function of the TOP response for the *probe* pion. Requiring $\log \mathcal{L}_X > \log \mathcal{L}_\pi$ we estimate $\mathcal{P}(\pi \to X)$, while to measure $\mathcal{P}(\pi \to \pi)$ we require $\log \mathcal{L}_\pi > \log \mathcal{L}_K$. The K_s mass distributions for four samples with different requirements on the likelihood values are shown in Figure 4. As expected, the K_s peak is clearly suppressed when the *probe* track is more compatible with either the kaon, proton, or electron hypothesis rather then the pion one.

Overall, the identification efficiencies for proton (not presented in this paper), kaon, and pion measured in the commissioning run are approximately 90% of those found in studies performed on simulation. Similar discrepancies are also present in fake-rate measurements, which are higher than the design value. Numerous studies are being performed to better understand these differences and reduce or eliminate them, as discussed in the next section.

5. Understanding the performance

The early analysis of the phase II data points to the preliminary calibrations used to reconstruct the data as the primary cause of the reduced particle identification capability. The TOP calibration consists of a time calibration, whose aim is to even

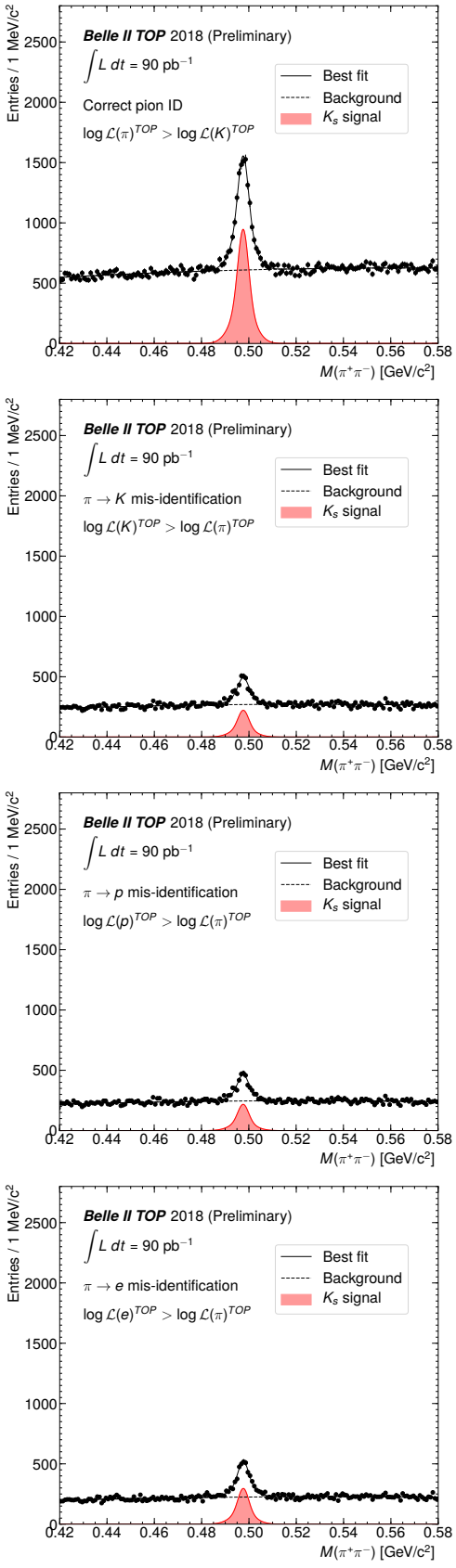

Figure 4: Mass distributions of the K_s candidates with four particle identification requirements. From top to bottom: $\log \mathcal{L}_\pi > \log \mathcal{L}_K$, $\log \mathcal{L}_K > \log \mathcal{L}_\pi$, $\log \mathcal{L}_p > \log \mathcal{L}_\pi$, and $\log \mathcal{L}_e > \log \mathcal{L}_\pi$.

the response of the 8192 MCP-PMT channels, and a geometrical alignment. The time calibration is performed in four consecutive steps, each depending on the previous steps [10]:

- *Time-base calibration*. This calibration aims to ensure the linearity of the front-end ASIC sampling array [11], and is performed by injecting electronic pulses in the front-end. After this calibration we measure, using a dedicated laser system [12], a single photo-electron time resolution per channel of approximately 120 ps.
- *Channel T_0 calibration*. Once the electronics have been properly calibrated, we compensate for the relative delays of the 512 channels within each TOP module. This calibration is performed by flashing the MCP-PMTs with a picosecond laser [12], and measuring the individual delay of each channel with respect to a reference channel.
- *Geometrical alignment and module T_0 calibration*. The laser calibration ensures that all the delays within each module are properly compensated, but does not correct for the delays between modules (namely, the relative delays between the reference channels of each module). The synchronization of the modules is expected to be done together with the geometrical alignment by an iterative procedure based on di-muon events from e^+e^- collisions [10].
- *Global T_0*. The Cherenkov photon time is measured with respect to the time of the original e^+e^- interaction. A very precise time reference is given by the accelerator Radio-Frequency (RF) clock, but to use it one needs to associate each event with the corresponding bunch crossing. This can be done by collecting all the tracks reconstructed in the event and, from the time of the hits in the TOP counter, fit the most probable interaction time. This algorithm has a resolution of $\approx$ 300 ps per event (to be compared with the SuperKEKB bunch crossing interval of 2 ns), corresponding to a bunch crossing identification efficiency of greater than 95%. For this procedure to be successful, one needs to calibrate the delay between the RF clock and the TOP (or in other words, the relative phase) to a precision equal to or smaller than the intrinsic uncertainty on the interaction time of 20 ps due to the bunch length. Any residual phase between the TOP and the RF clock will result in a net extra contribution to the TOP time measurement.

During and after the data taking, we found several issues in each of the above calibration steps. Firstly, residual non-linearities that, despite being rather small, significantly reduced the precision of the laser calibration. Then, the statistics of the di-muon collected were not sufficient to perform any of the track-based calibration to the required degree of precision. A first attempt to perform the geometrical alignment and module T_0 calibration was made but produced unreliable results due to the very limited $\mu^+\mu^-$ statistics. Since the time calibration of the modules with each other is critical for the TOP reconstruction, an alternative algorithm has been developed to use muons from the 2018 cosmic ray test dataset. The global T_0 calibration must be calculated for every run, but the statistics available still significantly limit its precision to $\approx$ 150 ps for an typical run, $\approx$ 300 ps for the shortest run and $\approx$ 30 ps for the longest. This is the largest contribution to the total time resolution of the TOP detector identified so far. All these effects, combined with a reduced hit reconstruction efficiency due to the early version of the front-end firmware used during phase II, and convoluted with all the effects from the preliminary tracking calibration, can explain the performance degradation we observe.

6. Future prospects

The Belle II experiment will resume the data taking in April 2019, after the installation of the silicon vertex detectors, and will continue it until July of the same year. Before the beginning of the data taking, several improvements to the TOP front-end settings have been made. A new firmware version has been deployed to increase the hit finding efficiency and we proceeded with a fine-tuning of the front-end ASIC parameters, that further increased the efficiency and improved the timing performance. As result of these modification, the precision of the time-base calibration has been improved.
The other calibrations have been improved as well. A more realistic modeling of the laser time distribution has been introduced increasing the quality of the channel T_0 calibration. A final re-analysis of the *phase II* data allowed to perform a first approximate geometrical alignment using Bhabha events instead of di-muons. The precision of the global T_0 is expected to increase as consequence of the improved tracking performance and the larger statistics that will be collected per each run in 2019.
An updated study of the TOP performance is expected for the late summer 2019.

References

[1] T. Abe *et al.* [Belle II Collaboration], arXiv:1011.0352 [physics.ins-det].
[2] E. Kou *et al.* [Belle II Collaboration], arXiv:1808.10567 [hep-ex].
[3] M. Akatsu *et al.*, Nucl. Instrum. Meth. A **440**, 124 (2000).
[4] T. Ohshima, ICFA Instrum. Bull. **20**, 2 (2000).
[5] K. Inami, Nucl. Instrum. Meth. A **595**, 96 (2008).
[6] K. Inami [Belle-II PID Group], Nucl. Instrum. Meth. A **766**, 5 (2014).
[7] K. Inami, Physics Procedia 37 (2012) 683 – 690.
[8] K. Matsuoka *et al.*, PoS PhotoDet2015 (2016) 028.
[9] M. Staric, Nucl. Instrum. Meth. A **639**, 252 (2011).
[10] M. Staric [Belle II TOP Group], Nucl. Instrum. Meth. A **876**, 260 (2017).
[11] D. Kotchetkov *et al.*, arXiv:1804.10782 [physics.ins-det].
[12] U. Tamponi, Nucl. Instrum. Meth. A **876**, 59 (2017).